Research article
Eurasian J. Bio. Chem. Sci. 2(2):47-51, 2019

Eurasian Journal of Biological and Chemical Sciences

Journal homepage: www.dergipark.org.tr/ejbcs

Thermal kinetics and thermodynamics of the dehydration reaction of $Mg_3(PO_4)_2 \cdot 22H_2O$

Fatma Tugce Senberber[1*], Emek Moroydor Derun[2]
*[*1]Nisantasi University, Faculty of Engineering and Architecture, Department of Civil Engineering, Istanbul, Turkey.*
[2]Yildiz Technical University, Faculty of Chemistry and Metallurgy, Department of Chemical Engineering, Istanbul, Turkey.

*Corresponding author : fatma.senberber@nisantasi.edu.tr; tsenberber@gmail.com
Orcid No: 0000-0002-3257-1524

Received : 25/07/2019
Accepted : 26/07/2019

Abstract: $Mg_3(PO_4)_2 \cdot 22H_2O$ lost its crystal water in the temperature range of 40 - 200°C and the calcined sample was identified as $Mg_3(PO_4)_2$, was a notable for its further treatments in optical and electrical applications. Dehydration process was studied using non-isothermal thermogravimetry (TG) applying model-fitting method. Different mechanism models (chemical reaction order, diffusion and phase interfacial reaction) were applied. The activation energies calculated for the dehydration reaction; and average of activation energy was found as 160 kJ/mol. The better kinetic model of the dehydration reaction for $Mg_3(PO_4)_2 \cdot 22H_2O$ was selected as F3 (chemical reaction - third order). The thermodynamic functions (ΔH, ΔG and ΔS) of the dehydration reaction were calculated by the activated complex theory and found that the process was endothermic, non-spontaneous and fast.

Keywords: Magnesium phosphate, decomposition kinetic, thermal behaviour, thermodynamic

1. Introduction

Chemically bonded phosphate ceramics generally occur with the reaction of a metal cation and phosphate ion. They can be classified according to the metal cation in structure. Although being cementitious materials, magnesium phosphates have similar features and with ceramics. They are quick-setting and hard materials. The phosphate anion in the structure makes the ceramic biocompatible (Yu et al.,2017; Yu and Jiang, 2018). They can be used novel biomaterial designs or can be added to calcium phosphate to increase hardness (Wu et al., 2008). Therefore, magnesium phosphates are preferred in dental and bone restorations, implants, medicine and agriculture (Lu and Chen, 2016; Boonchom, 2009; Qiao et al., 2010; Yang et al., 2000; Rouzic et al., 2017; Kongshaug et al., 2001). Also, this type of phosphate has dissolubility in water, chemical and thermal resistance. This situation makes them useful for anti-corrosive coating and surfaces (Pokorny et al., 2016; Zhang and Tang, 2015).

Magnesium phosphates can be synthesized by chemical precipitation, hydrothermal, solid-state, microwave or biosynthesis methods (Yu et al., 2016; Zhou et al., 2012). Thermal-treated magnesium phosphates can be used as catalyst in organic processes of biomass applications. (Boonchom, 2009; Gopinath et al.,2015; Debnath et al.,2016; Aramendia et al.,1999). The dehydrated forms of magnesium phosphate, $MgHPO_4$ and $Mg_3(PO_4)_2$, are notable for their dielectric, ferroelectric, piezoelectric and optical features (Assaaoudi et al., 2007; Zhang et al., 2016). The chemical structure and textural features of phosphates are notable for these usage areas. For this purpose, the studies on thermal behaviour, thermal decomposition mechanism and thermodynamic functions of ΔH, ΔG and ΔS are important in the manufacturing processes this purpose (Kanazawa et al., 1979; Sadiq et al.,2015; Sadiq et al., 2008). $MgHPO_4 \cdot 3H_2O$, $MnHPO_4 \cdot H_2O$ and $LiMnPO_4$ are the characterized forms of metal phosphates by thermal kinetic and thermodynamic studies (Boonchom, 2009; Sronsri and Boonchom 2018, Boonchom and Danvirutai 2008).

In this research, it is aimed to explain the mechanism, kinetics and thermodynamics of the decomposition of $Mg_3(PO_4)_2 \cdot 22H_2O$ using thermal analyses techniques. Thermal decomposition process of mineral was interpreted by Coats-Redfern non-isothermal kinetic method. The thermal kinetic (E_a, A, n, mechanism and model) and thermodynamic (ΔH, ΔS and ΔG) parameters of the dehydration reaction of $Mg_3(PO_4)_2 \cdot 22H_2O$ were determined.

2. Materials and Method

2.1. Mineral preparation and characterization

Hydrates forms of magnesium phosphates can be synthesized in basic hydrothermal conditions (Mousa,

2010). Magnesium source of magnesium oxide (MgO) and phosphorus source of phosphoric acid were reacted under magnetic stirring at room temperature for 1 hour. pH value was determined 10. The prepared white powders were filtered and dried at 40ºC.

The sample was identified by X-ray diffraction analysis (XRD). A Philips PANalytical XPert Pro X-ray diffractometer was used at 40 mA, 45 kV and Cu-Ka radiation in the 2θ range of 5°–60°. The vibrational modes of sample were analysed by a PerkinElmer Spectrum One FT-IR with a universal attenuation total reflectance (ATR) sampling accessory with a diamond/ZnSe crystal. Thermal behaviour of sample was studied between the temperature ranges of 30–500°C with a Perkin Elmer Diamond TG/DTG. Five different heating rates (5, 10, 15, and 20°C/min) were applied under the nitrogen atmosphere.

The prepared sample was placed in a Protherm MOS 180/4 high-temperature furnace in nitrogen flowing (5 ml/min) atmosphere. Calcined sample was further analysed by XRD.

2.2. Thermal dehydration kinetics and thermodynamic analysis

Thermal solid-state decomposition in solid-gas system of the single-crystalline compound was given in Equation 1. For a hydrate mineral, the escaping gas was water and this process was called dehydration.

$$A_{solid} \rightarrow B_{solid} + C_{gas} \quad (1)$$

Thermal behaviour can be explained by using the thermogravimetric data. The activation energy (E_a, kJ/mol), exponential factor (A) and reaction order (n) of dehydration reaction were calculated by using the Coats-Redfern Method. Integrated and linear forms of Coast Redfern were given in Equations 2 and 3. In this method, the E_a and A can be calculated from the slope and intercept of the $\ln[g(\alpha)/T^2]$ vs 1/T plot, respectively (Lopez et al., 2015; Boonchom and Puttawong, 2010).

$$g(\alpha) = \int_0^{\alpha} \frac{d(\alpha)}{f(\alpha)} = \frac{A}{\beta}\int_{T_0}^{T} \exp\left(-\frac{E_a}{RT}\right) dT \quad (2)$$

$$\ln\left(\frac{g(\alpha)}{T^2}\right) = \ln\left(\frac{AR}{E_a\beta}\right) - \frac{E_a}{RT} \quad (3)$$

where α is the degree of conversion, f(α) is a function of conversion according to the reaction mechanism, g(α) is a kinetic function of different reaction mechanisms which is obtained from integration of f(α). R is the gas constant (8.314×10^{-3} kJ/mol), T is the absolute temperature, and β is the heating rate (°C/min). The solid-state reaction mechanisms and models were listed in Table 1.

Table 1. Reaction mechanisms, model names and functions of f(α) and g(α)

Reaction Mechanism	Model Name	Model Code	f(α)	g(α)
Chemical reaction order	1st order	F1	1-α	-ln(1- α)
	2nd order	F2	$(1- \alpha)^2$	$1-(1- \alpha)^2$
	3rd order	F3	$(1- \alpha)^3$	$(1-(1- \alpha)^3)/2$
Diffusion	One dimensional	F4	1/2α	α^2
	Two dimensional	F5	$-(\ln(1- \alpha))^{-1}$	α+(1- α).ln(1- α)
Phase interfacial reaction	Shrinkage geometrical column	F6	$2(1- \alpha)^{1/2}$	$1-(1- \alpha)^{1/2}$
	Shrinkage geometrical spherical	F7	$2(1- \alpha)^{2/3}$	$1-(1- \alpha)^{1/3}$

The thermodynamic factors of enthalpy change (ΔH), Gibbs energy change (ΔG), and entropy change (ΔS) were calculated by using the obtained thermal kinetic parameters of A and E_a for the best-fitted reaction mechanism. The equations used in thermodynamic calculations were given in Equations 4-6 (Naqvi et al., 2018).

$$\Delta H = E_a - RT \quad (4)$$

$$\Delta G = E_a + RT_m \ln\left(\frac{K_B T}{hA}\right) \quad (5)$$

$$\Delta S = \frac{\Delta H - \Delta G}{T_m} \quad (6)$$

where K_B is Boltzmann constant (1.381×10^{-23} m^2kg/s^2K), T_m is the temperature at which maximum decomposition occurs (peak point of the DTG curve) and h is the plank constant (6.626×10^{-34} m^2kg/s^2).

3. Results

3.1. XRD results

XRD patterns of un-calcined and calcined samples were presented in Figure 1. The prepared sample was identified as Magnesium Phosphate Hydrate ($Mg_3(PO_4)_2\cdot22H_2O$) with the powder diffraction file number of 00-044-0775 (Figure 1a). The magnesium phosphate hydrate was calcined at 500°C. The calcined sample was identified as Farringtonite ($(Mg_3(PO_4)_2)$) with the powder diffraction file number of 00-033-0876 (Figure 1b).

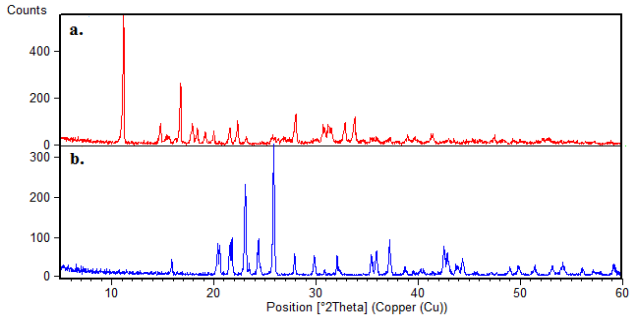

Figure 1. XRD patterns of a. un-calcined and b. calcined samples

3.2. FT-IR results

FT-IR spectrum of $Mg_3(PO_4)_2 \cdot 22H_2O$ was presented in Figure 2. The OH^{-1} vibrations in hydrate structure and H-O-H vibrations were seen 3450 cm^{-1} and 1655 cm^{-1}, respectively. The characteristic band values for the PO_4^{-3} was seen at the band value of 1066 cm^{-1}. The band values at the 715 cm^{-1} can be explain with the bending of $PO_2(OH)$. The out of plane of phosphate ion was observed at 578 cm^{-1}.

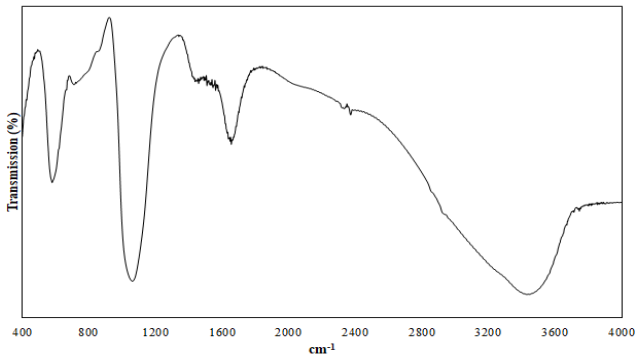

Figure 2. FT-IR spectrum of $Mg_3(PO_4)_2 \cdot 22H_2O$

3.3. Thermal analyses results

Dehydration behaviour of magnesium phosphate hydrate was investigated by using thermal analyses techniques. Thermal analyses result of $Mg_3(PO_4)_2 \cdot 22H_2O$ were given Table 2. TG/DTG curves of $Mg_3(PO_4)_2 \cdot 22H_2O$ for different heating rates were given in Figure 3. According to the thermal curves, dehydration process occurred in the temperature range of 40–200°C and mass was determined as approximately %55.5. The peak temperature of DTG curves were seen between 67 and 79°C.

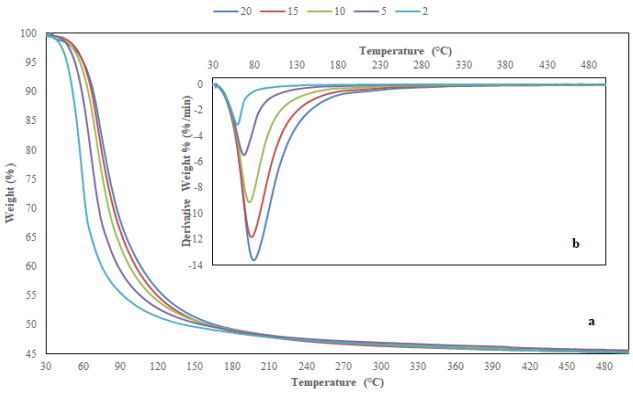

Figure 3. TG/DTG curves of $Mg_3(PO_4)_2 \cdot 22H_2O$ a. TG and b. DTG

3.4. Thermal kinetic results

Coast Redfern non-isothermal kinetic method was applied for the calculation of thermal kinetic parameters of E_a and A. Mechanisms of chemical reaction order (F1, F2 and F3), diffusion (F4 and F5) and phase interfacial reaction (F6 and F7) were used in thermal kinetic modelling. The calculated kinetic parameters at the different heating rates were given Table 3.

Correlation factors (R^2) were observed between 0.7882 and 0.9942. The third order of chemical reaction was selected as best fitted mechanism, because of the highest linearity. R^2 values varied between 0.9903 and 0.9942 for reaction model of F3. In this reaction model, the activation energies (E_a) were found in the range of 123.01 – 170.97 kJ/mol. Exponential factors (A) changed in the range of 1.24×10^{35} - 3.47×10^{18} for the F3 model. Thermal kinetic parameters of E_a and A showed a falling tendency with the increasing heating rates, in all models.

3.5. Thermodynamic results

Thermodynamic parameters of ΔH (kJ/mol), ΔG (kJ/mol) and ΔS (kJ/mol×K) were calculated at different heating rates by using the best-fitted kinetic model (F3) as shown in Table 4. Acceptable differences were observed between the estimated thermodynamic parameters varying heating rates.

ΔH values were found in the range of 120.08 – 221.55 kJ/mol thermal dehydration of magnesium phosphate hydrate. ΔG and ΔS values were determined in the range of 82.50 – 84.74 kJ/mol and 0.1 – 0.248 kJ/mol×K, respectively.

Table 2. Thermal analyses result of $Mg_3(PO_4)_2 \cdot 22H_2O$

β (°C/min)	$T_{initial}$ (°C)	T_{final} (°C)	T_{max} (°C) (DTG)	Mass loss (%)
5	46.28	107.76	67.51	55.49
10	48.51	120.12	73.79	55.59
15	50.97	137.56	76.49	55.60
20	52.16	144.98	79.16	55.73

Table 3. Calculated kinetic parameters for Coast Redfern method

Model Code	β (°C/min)	R^2	E_a (kJ/mol)	A	Model Code	β (°C/min)	R^2	E_a (kJ/mol)	A
F1	5	0.8992	76.04	7.39×10^{10}	*F5*	5	0.8149	119.13	5.64×10^{16}
	10	0.9065	68.84	6.26×10^{9}		10	0.8265	109.53	1.56×10^{15}
	15	0.8774	57.26	1.04×10^{8}		15	0.7899	90.83	1.88×10^{12}
	20	0.8752	54.15	3.84×10^{7}		20	0.7882	86.24	3.82×10^{11}
F2	5	0.9804	117.73	4.66×10^{17}	*F6*	5	0.8291	61.28	1.32×10^{8}
	10	0.9827	105.21	4.67×10^{15}		10	0.8386	55.87	2.32×10^{7}
	15	0.9716	89.18	1.44×10^{13}		15	0.7987	45.93	7.16×10^{5}
	20	0.9706	84.41	2.77×10^{12}		20	0.7954	43.42	3.33×10^{5}
F3	5	0.9942	170.97	1.80×10^{26}	*F7*	5	0.8019	115.41	9.14×10^{12}
	10	0.9926	151.54	1.14×10^{23}		10	0.8156	107.07	6.84×10^{10}
	15	0.9911	129.94	4.19×10^{19}		15	0.7838	89.77	5.25×10^{7}
	20	0.9903	123.01	3.47×10^{18}		20	0.7836	85.59	3.54×10^{6}
F4	5	0.8422	136.18	8.14×10^{12}					
	10	0.8556	126.03	1.30×10^{9}					
	15	0.8293	107.06	1.92×10^{6}					
	20	0.8287	101.94	1.85×10^{5}					

Table 4. Calculated thermodynamic parameters for the best-fitted kinetic model

Model Code	β (°C/min)	ΔH (kJ/mol)	ΔG (kJ/mol)	ΔS (kJ/mol×K)
F3	5	168.14	83.56	0.248
	10	148.65	83.80	0.187
	15	127.03	84.69	0.121
	20	120.08	84.74	0.100

4. Discussion

Removal of 22 moles of crystal water was occurred during the dehydration. In the light of XRD and thermal analyses, the probable reaction for the dehydration process were given in Equation 7.

$$Mg_3(PO_4)_2 \cdot 22H_2O(s) \xrightarrow{heat} Mg_3(PO_4)_2(s) + 22H_2O(g) \quad (7)$$

The differences in calculated activation energies can be explained with the low linearity in correlation and lack of the reaction order in other selected models. Due to the lower linearity for the reaction models of diffusion and phase interfacial (F4 – F7), these models were not suitable for the explanation of reaction model.

Exponential factor (A) was generally associated with the number of times molecules hit in the orientation necessary to cause a reaction (Naqvi et al., 2018). In general, the low and high factors could be explained with the tight and loose complexes, respectively. The thermal dehydration reaction of $Mg_3(PO_4)_2 \cdot 22H_2O$ may be classified as loose complex, which corresponds to the removal of crystallization water. These results are compatible with thermal analysis, which confirm that the decomposition product as tri-magnesium phosphate anhydrous $Mg_3(PO_4)_2$.

Positive value of ΔH indicated the propellent power of temperature increase, which meant the endothermic reaction (Boonchom 2008). Positive value of ΔG showed that dehydration process of $Mg_3(PO_4)_2 \cdot 22H_2O$ was non-spontaneous processes and were necessary to connect with the introduction of heat. The positive value ΔS can be interpreted as the decomposition of a malleable complex which means a fast step (Lopez et al., 2015; Naqvi et al., 2018; Boonchom, 2008).

5. Conclusions

Crystal water of magnesium phosphate hydrate ($Mg_3(PO_4)_2 \cdot 22H_2O$) removed by a single step between the temperatures of 40 and 200°C and the heat-treated product was $Mg_3(PO_4)_2$, significant for its optical and electrical applications. Dehydration process was studied using Coats-Redfern non-isothermal kinetic method and activation energies determined for the different mechanism models. Mechanism models of chemical reaction order (1st, 2nd and 3rd), diffusion (one dimensional and two dimensional) and phase interfacial reaction (shrinkage geometrical column and shrinkage geometrical spherical) were applied. According to the higher linearity in thermal calculations correlation, reaction mechanism can be explained with the 3rd order chemical reaction (F3) for the one-step dehydration reaction of $Mg_3(PO_4)_2 \cdot 22H_2O$. The thermodynamic functions (ΔH, ΔG and ΔS) of the dehydration reaction were calculated by the activated complex theory and found that the process was endothermic, non-spontaneous and fast.

Acknowledgements

This research did not receive any specific grant from funding agencies in the public, commercial, or not-for-profit sectors.

Authors' contributions: F.T.S and E.M.D. contributed to the design and implementation of the research, to the analysis of the results and to the writing of the manuscript.

Conflict of interest disclosure:

The authors have no conflict of interest to study.

References

Aramendia MA, Borau V, Jimenez C, Marinas JM, Romero FJ 1999. Synthesis and characterization of magnesium phosphates and their catalytic properties in the conversion of 2-hexanol. Journal of Colloid and Interface Science, 217: 288–298.

Assaaoudi H, Fang Z, Butler IS, Ryan DH, Kozinski JA 2007. Characterization of a new magnesium hydrogen orthophosphate salt, $Mg_{3.5}H_2(PO_4)_3$, synthesized in supercritical water. Solid State Sciences 9: 385 – 393.

Boonchom B 2008. Kinetics and Thermodynamic Properties of the Thermal Decomposition of Manganese Dihydrogenphosphate Dihydrate. Journal of Chemical Engineering Data, 53: 1533–1538.

Boonchom B 2009. Kinetic and thermodynamic studies of $MgHPO_4 \cdot 3H_2O$ by non-isothermal decomposition data. Journal of Thermal Analysis and Calorimetry, 98: 863–871.

Boonchom B, Danvirutai C 2008. A simple synthesis and thermal decomposition kinetics of $MnHPO_4 \cdot H_2O$ rod-like microparticles obtained by spontaneous precipitation route. Journal Of Optoelectronics And Advanced Materials, 10(3): 492 – 499.

Boonchom B, Puttawong S 2010. Thermodynamics and kinetics of the dehydration reaction of $FePO_4 \cdot 2H_2O$, Physica B, 405: 2350–2355.

Debnath S, Saxena SK, Nagabhatla V 2016. Facile synthesis of crystalline nanoporous $Mg_3(PO_4)_2$ and its application to aerobic oxidation of alcohols. Catalysis Communications 84: 129–133.

Gopinath P, Ramalingam V, Breslow R 2015. Magnesium pyrophosphates in enzyme mimics of nucleotide synthases and kinases and in their prebiotic chemistry. Proceedings of the National Academy of Sciences of the United Sciences, 112(39): 12011–12014.

Kanazawa T, Umegaki T, Shimizu M 1979. The synthesis of Mg3(PO4)2·8H2O and its polymorphism. Bulletin of the Chemical Society of Japan, 52(12): 3713–3717.

Kongshaug KO, Fjellvag H, Lillerud 2001. The synthesis and crystal structure of a hydrated magnesium phosphate $Mg_3(PO_4)_2 \cdot 4H_2O$. Solid State Sciences, 3: 353–360.

Lopez FA, Tayibi H, Diaz IG, Alguacil FJ 2015. Thermal dehydration kinetics of phosphogypsum. Materiales de Construction, 65(319): 1-14.

Lu X, Chen B 2016. Experimental study of magnesium phosphate cements modified by metakaolin. Construction and Building Materials, 123: 719–726.

Mousa S 2010. Study on synthesis of magnesium phosphate materials. Phosphorus Research Bulletin, 24: 16 – 21.

Naqvi SR, Tariq R, Hameed Z, Ali I, Naqvi M, Chen WH, Ceylan S, Rashid H, Ahmad J, Taqvi SA, Shahbaz M 2018. Pyrolysis of high ash sewage sludge: kinetics and thermodynamic analysis using Coats-Redfern method, Renewable Energy, (*In Press*) doi: 10.1016/j.renene.2018.07.094

Pokorny P, Tej P, Szelag P 2016. Discussion about magnesium phosphating. Metalurgija, 55(3): 507–510.

Qiao F, Chau CK, Li Z 2010. Property evaluation of magnesium phosphate cement mortar as patch repair material. Construction and Building Materials, 24: 695–700.

Rouzic M, Chaussadent T, Platret G, Stefan L 2017. Mechanisms of k-struvite formation in magnesium phosphate cements. Cement and Concrete Research, 91: 117–122.

Sadiq M, Abdennouri M, Barka N, Baalala M, Lamonier C, Bensitel M 2015. Influence of the Crystal Phase of Magnesium Phosphates Catalysts on the Skeletal Isomerization of 3,3-dimethylbut-1-ene. Canadian Chemical Transactions, 3(2): 225–233.

Sadiq M, Bensitel M, Lamonier C, Leglise J 2008. Influence of the nature of precipitating basic agent on the synthesis of catalytic magnesium phosphate materials. Solid State Sciences, 10: 434–437.

Sronsri C, Boonchom B 2018. Determination of thermokinetic parameters and thermodynamic functions from thermoforming of $LiMnPO_4$. Journal of Thermal Analysis and Calorimetry, 134(3): 1575 – 1587.

Wu F, Wei J, Guo H, Chen F, Hong H, Liu C 2008. Self-setting bioactive calcium–magnesium phosphate cement with high strength and degradability for bone regeneration. Acta Biomaterialia, 4: 1873–1884.

Yang Q, Zhu B, Wu X 2000. Characteristics and durability test of magnesium phosphate cement-based material for rapid repair of concrete. Materials and Structures, 33: 229–234.

Yu C, Wu Q, Yang J 2017. Effect of seawater for mixing on properties of potassium magnesium phosphate cement paste. Construction and Building Materials, 155: 217–227.

Yu X, Jiang J 2018. Mineralization and cementing properties of bio-carbonate cement, bio-phosphate cement, and bio-carbonate/phosphate cement: a review. Environmental Science and Pollution Research, 25: 21483–21497.

Yu XN, Qian CX, Sun LZ 2016. Chemosynthesis of nano-magnesium phosphates and its characterization. Digest Journal of Nanomaterials and Biostructures, 11(4): 1099–1103.

Zhang S, Li L, Lv X 2016. Synthesis and characterization of a novel $Mg_3(PO_4)_2$ ceramic with low dielectric constant. Journal of Materials Science: Materials in Electronics, DOI: 10.1007/s10854-016-5703-y

Zhang Z, Tang W 2015. Tunable Blue–Red Emission and Energy-Transfer Properties of $Mg_3(PO_4)_2:Eu^{2+},Mn^{2+}$ Phosphors. Eyropen Journal of Inorganic Chemistry, 2015: 3940–3948.

Zhou H. Luchini TJF, Bhaduri SB 2012. Microwave assisted synthesis of amorphous magnesium phosphate nanospheres. Journal of Materials Science: Materials in Medicine, 23:2831–2837.